Transcriptional Profiling of Primate Central Nucleus of the Amygdala Neurons to Understand the Molecular Underpinnings of Early Life Anxious Temperament

Supplement 1

Supplemental Methods

Animals

All animals were phenotyped for AT as described below and brains for the subset of 47 animals were collected for LCM and RNA-Seq analysis. The majority of these 47 animals were of Indian ancestry, with a subset that were a hybrid of Indian and Chinese ancestry. Monkeys were humanely euthanized by anesthetizing with ketamine (at least 15 mg/kg, IM) followed by sodium pentobarbital. Two C57BL/6J mice, two KO; B6;129X1-*Prkcd*^{tm1Msg}/J mice, and two additional rhesus monkey brains were used to characterize antibodies. Triple-labeling immunofluorescence and stereology was performed on three C57BL/6J mice (WT, age=p21) and three rhesus monkey brains (average age=3.1 yrs). Triple-labeling immunofluorescence for the retrograde traced issue was performed on six monkeys (*Macaca fascicularis* and *Macaca nemestrina*; average age=2-3 years). All procedures were approved by the Committee on the Ethics of Animal Research of the University of Wisconsin and of the University of Rochester.

Animal Housing

Veterinary care, supported by clinical laboratories, was available at the both the Wisconsin National Primate Center and the Harlow Center for Biological Psychology, as well as the University of Rochester 24 hours a day, seven days a week. Monkeys were mother-reared, and pair-housed in a room containing multiple cages, to facilitate social housing. Monkeys experienced a 12-hour light/dark cycle, received food 1-2 times per day and water was available *ad libitum*. Monkeys experienced enrichment activities such as toys, foraging devices, tactile devices, audio, television and snack foods such as fruit at least once per day. Mice were ordered from The Jackson Laboratory (Bar Harbor, ME) and were group housed at the Wisconsin Psychiatric Institute and Clinics for at least 7 days before experimentation. Mice experienced a 12-hour light/dark cycle and were given *ad libitum* access to food and water. Any discomfort, distress, pain, and injury were minimized by the appropriate use of anesthetic and analgesic drugs under the direction and supervision of the veterinary staff.

Anxious Temperament Phenotyping

Anxious temperament (AT) phenotyping was performed between 8:00am and 11:00am to control for time of day. To assess individual differences in AT, we used the mildly threatening no eye contact condition (NEC) of the human intruder paradigm (Figure S1A; 1-4) During this 30 minute condition, a human intruder presents their profile to the monkey ensuring to not make eye contact (2, 4). This condition is unique in that it elicits behaviors that reflect uncertainty in relation to potential threat. High levels of AT are characterized by increased plasma cortisol, increased freezing, and decreased cooing occurring during the NEC condition (4). Freezing is defined as a 3 second period characterized by lack of body movement that is accompanied by a tense body posture and sometimes slow movements of the head. Coo vocalizations are vocalizations made by rounding and pursing the lips characterized by an increase, then decrease in frequency and intensity. The duration of freezing was assessed for six, consecutive, 5-minute blocks. The average freezing duration across the blocks was log transformed to ensure a normal distribution. Cooing frequency was similarly averaged across the blocks and square root transformed. Blood

samples for cortisol assessment were collected by femoral venipuncture at the end of the 30-minute NEC exposure. Blood withdrawal was collected when monkeys were placed in a special cage used to limit their locomotor capacities and a leg could be accessed for venipuncture. FDG PET imaging was performed at the end of the NEC period but is not included in this paper. Because cortisol is affected by time of day, cortisol levels were residualized for the time of day of sample collection. Freezing, cooing and cortisol were also residualized for age. For the 47 animals, AT scores were calculated by taking the average of their combined residualized and standardized freezing, cooing, and cortisol values. When examining the AT scores of these 47 animals in relation to the larger superset, we found that they had a similar distribution, spanning approximately +/- 1 std from the mean of the larger cohort (Figure S1B). Behavioral data was analyzed using scripts written in python 3.6 (Python Software Foundation, https://www.python.org/) using IPython (5) that utilized pandas (6), scipy (7), and statsmodels (8) modules.

Cortisol Assessment

Plasma samples were assayed for cortisol in duplicate using the DPC Coat-a-count radioimmunoassay (Siemens, Los Angeles, CA). The inter-assay CV%s calculated for a low and a high control were based on 21 assays. The low control had an average value of 48.4 µg/dL and a CV% of 7.0 and the high control had an average value of 128.3 µg/dL and a CV% of 7.0. The limit of detection defined by the lowest standard was 1 µg/dL.

NeuN Rapid Staining Protocol

Brain slabs used for laser capture microdissection (LCM) were counterbalanced for hemisphere across animals. The slab containing the CeL was selected for each animal. Acetylcholinesterase (AChE) staining was used to confirm that the slab contained the amygdala (Figure S2B). In cases in which the amygdala was contained in two slabs, both were used. Tissue was sectioned on a cryostat, mounted on LCM slides, and placed in a -80^{o}C freezer until staining. All staining was completed in an RNA-free environment and all steps were done on ice unless otherwise specified. LCM slides were removed from the -80^{o}C freezer and thawed on a metal block for 30 seconds. Slides were fixed in acetone for 3 minutes at -20^{o}C and then washed in PBS with 0.1% Triton x-100 (PBS-T) for 2 minutes. The tissue was stained with a neuron specific protein (NeuN) antibody (MAB377, Millipore, Burlington, MA) at a 1:200 dilution for 25 minutes at room temperature. Slides were submerged in PBS-T for 2 minutes and incubated in an HRP secondary antibody (PI-2000, Vectorlabs, Burlingame, CA) at 1:250 for 30 minutes at room temperature. Slides were then washed in PBS-T for 2 minutes and dipped in regular PBS for 30 seconds. Tissue was incubated in ImmPACT VIP peroxidase substrate (SK-4605, Vectorlabs) for 7-10 minutes before washing in DEPC-treated H_2O for 5 minutes. Finally, the slides were dipped into 95% ethanol briefly before being dehydrated for 10-20 seconds each in 95% ethanol, 100% ethanol, and xylene. Slides were dried in a fume hood for 5 minutes before being transported to the laser capture microscope.

Laser Capture Microdissection Protocol

For dissection, neurons were identified at 20x magnification and a circle that was approximately 850 µm^2 was drawn around each neuron and neurons were then dissected with a laser and fell into the lid of a microfuge tube (PCR-05-C, Axygen, Corning, NY) filled with 40uL of lysis buffer. After all neurons from the slide were captured, an additional 10uL of lysis buffer was added to the microfuge tube. The tube was vortexed on high for 30 seconds before being placed on dry ice. Tubes containing neuronal RNA were only used if at least 80% of the cells captured were identified as coming from the CeL, confirmed by overlying each LCM slide image with its adjacent AChE slide. From our collection, we established 3 categories: 100% CeL cells, 80-99% CeL cells, and <80% CeL cells. Those slides that were <80% CeL cells were not used for RNA-Seq. To determine the “CeL neuron accuracy” for each animal, we calculated the proportion of the number

of slides that contained 80-99% of CeL neurons out of total slides used for RNA-Seq (X 80-99% slides / (X 80-99% slides + Y 100% slides); Figure S2B). AChE images were assigned a bregma value that most closely matched that AchE image in the Paxinos Atlas (9). A "weighted average bregma" value was calculated for each animal by multiplying the bregma value for each slide by the number of cells captured for in that slide and taking an average (Figure S3B). For half of the animals (n=29), RNA from one slide was extracted and run on an Agilent Bioanalyzer to determine 18S and 28S peaks and RNA integrity numbers (average = 4, std = 0.75).

RNA Sequencing Data Analysis

All data were analyzed using either scripts written in python or R. OLS regression and permutation testing were performed in python 2.7. For DESeq2 analyses, data were manually filtered and outliers removed based on a cook's D distance of 3.8, calculated using a quantile function (qf) distribution as recommended by DESeq2 (10). For the heatmap (Figure 2A), the ward method of unsupervised clustering was performed in scripts written in python 3.6 (Python Software Foundation, https://www.python.org/) using the seaborn (version 0.0.9, https://seaborn.pydata.org) module which utilizes matplotlib (11). Gene expression values in the heatmap are presented as log2 transformed, min-max scaled values. Gene expression values in scatterplots are quantile normalized, log2 transformed, and residualized for covariates.

Non-parametric Multiple Testing Correction

For each gene, a permutation test was performed to obtain a non-parametric empirical p-value for the squared value of the correlation coefficient between AT and the log-transformed residualized value from our model covariates (age and accuracy ratio). In each simulation the AT parameters were shuffled, and the correlation coefficient was calculated and compared to our real correlation coefficient value. The simulation was carried out until the null squared correlation exceeded the observed parameter at least ten times (a numerator of between 10,000 and 30 million iterations), and this value was used to calculate the empirical p-value. Empirical p-values were then FDR corrected using then Benjamin-Hochberg procedure.

Weight Gene Co-expression Network Analysis

Iterative weighted gene co-expression network analysis (iWGCNA) was performed to identify groups of related genes that may fall within the same molecular pathway (12). CeL LCM transcripts were limited to those expressed in at least 50% of animals with a minimum expression level of 10 transcripts for those animals expressing the gene. Gene expression values were correlated and then taken to a power β to reach approximate scale-free topology. This was determined using the WGCNA package in R (13) and was found to be 10. Signed co-expression networks were constructed that had a minimum module size of 15 genes and a minimum kME value of 0.4. Genes that did not form strong associations with other genes were considered unclassified and were removed from further analyses. Modules were tested to determine whether they were significantly related to AT or its components using a model that included CeL neuron accuracy and age at ToD as covariates and p-values were FDR corrected. All analyses were written in python 3.6 (Python Software Foundation, https://www.python.org/) using scipy, seaborn (version 0.0.9, https://seaborn.pydata.org), matplotlib (11), and pandas (7).

Immunohistochemistry: Tissue collection, PKCδ antibody characterization, staining protocols, and stereological analysis

To characterize the PKCδ antibodies, a brain from one additional monkey and brains from a wildtype (WT; C57BL/6J; stock 000664, Jackson Laboratories, Farmington, CT) and a PKCδ knockout (KO; B6;129X1-*Prkcd*^{tm1Msg}/J; stock 028055, Jackson Laboratories) mouse were used. After characterization, perfused brains from three monkeys and three mice were used for between species comparison of PKCδ in the CeL. Animals were perfused using a standard protocol (15).

Brains were extracted, fixed overnight in 4% paraformaldehyde, cryoprotected in 30% sucrose, sectioned at 40-50μm and stored in cryoprotectant solution (30% ethylene glycol and 30% sucrose in 0.1 M phosphate buffer) at −20 °C (16).

PKCδ Antibody Characterization for Use in Rhesus Monkey Tissue

Three PKCδ antibodies (Key Resources) were assessed by staining both WT and PKCδ KO tissue using a standard immunohistochemistry protocol (see below). Those antibodies with specific binding to the PKCδ protein, were used in subsequent immunofluorescence experiments (Figure S4). The same antibodies were used to test for PKCδ staining in the monkey. To characterize specificity of PKCδ in monkey tissue, each antibody was preabsorbed with PKCδ peptide. Ten-fold molar excess of the PKCδ purified peptide was added to each antibody at their respective dilutions (Key Resources). The antibody-antigen mixture incubated for 36 hours at 4°C with mild agitation. The mixture was spun at 16,000g for 30 minutes. The resulting supernatant was pipetted into a clean vial and used in place of the primary antibody in the immunohistochemistry protocol.

Immunohistochemistry Protocol

Tissue from one mouse and monkey were stained together and all tissue was stained using the same lot of antibodies (Key Resources) and blocking serums. All tissue was removed from cryoprotectant solution 24 hours before staining and rinsed at least 3 times in 1x PBS. Primary antibodies were diluted in 1x PBS with 0.3% Triton x-100 and tissue was incubated overnight at room temperature. All secondary antibodies were made in 5% donkey serum. Fluorescent antibodies were also filtered through a 0.45μm filter to improve background staining.

Antibody characterization experiments were completed first and all staining was visualized using 3,3'-Diaminobenzidine (DAB). Tissue was incubated in 5% donkey serum (017-000-121, Jackson ImmunoResearch Laboratories, West Grove, PA) for 1 hour at room temperature. Tissue was subsequently washed three times in 1x PBS before being placed in PKCδ antibody overnight at room temperature. The following day, tissue for the antibody characterization experiments was washed in 1x PBS and incubated in an HRP conjugated secondary antibody diluted with blocking serum at 1:250 for 1 hour at room temperature. Tissue was then washed and incubated with ImmunoPact DAB (SK-4105, Vector Laboratories) for visualization of staining. Tissue was then mounted, left to dry overnight and then dehydrated in 75%, 95%, 100% ethanol solutions and xylene before being cover slipped. Images were captured at 1.25x, 5x and 20x magnification on a Leica LMD6500 microscope.

For triple labeling immunofluorescence, tissue was incubated serially in each antibody to avoid background. The staining protocols for the tissue used in the NeuN, PKCδ, and SST triple labeling experiment and the tissue used in the retrograde tracing experiment were the same. For the stereology experiment, tissue was first incubated in NeuN antibody overnight at room temperature, followed by 1x PBS washes and AlexaFluor 647 donkey anti-mouse secondary incubation for 1 hour at room temperature. For the retrograde tracing experiment, tissue was first incubated in anti-rhodamine, anti-WGA, or anti-fluorescein antibody overnight at room temperature, followed by 1x PBS washes and AlexaFluor 568 donkey anti-mouse secondary or AlexaFluor 488 donkey anti-goat secondary incubation for 1 hour at room temperature. Tissue was rinsed three times in 1x PBS and incubated in PKCδ antibody (1:200, Thermo Fisher) at room temperature for 24 hours for the mouse tissue and 48 hours for the monkey tissue. The following day tissue was washed three times in 1x PBS, incubated in AlexaFluor 488 donkey anti-rabbit for 1 hour at room temperature, washed three times in 1x PBS, and incubated in SST primary antibody for 72 hours to improve antibody penetration through the tissue. On the final day of staining, tissue was washed three times in 1x PBS and incubated in AlexaFluor 568 donkey anti-

goat for 1 hour at room temperature before being washed in 1x PBS, incubated for 5 minutes in DAPI, mounted on slides, and coverslipped with Prolong Gold AntiFade Mountant (P36930, Thermo Fisher).

Anatomical Boundaries of the Amygdala

The anatomical boundaries of the amygdala nuclei are well established in rodents (17). We delineated the lateral division of the central nucleus in mouse tissue based on previously described work (18) and corroborated this with adjacent sections stained for AChE. In rhesus monkeys the nomenclature and anatomical boundaries have been previously described (19, 20). We used these descriptions to delineate the anatomical boundary for the lateral division of the central nucleus (CeL) in the rhesus monkey. We used the nomenclature system in the Paxinos atlas (9) for rhesus monkeys (Figure 3A) and for consistency, extend this nomenclature to the mouse (Figure 3A).

Imaging Protocol and Stereological Analysis

For the NeuN, PKCδ, and SST triple labeling experiment, the optical fractionator method was used to determine the total number of neurons, PKCδ+ neurons, SST+ neurons, and double labeled neurons in the CeL (21, 22). Eight to ten sections per monkey and 4 sections per mouse through the anterior-posterior extent of the CeL was used and the first section was randomly selected within the first 6 (in mouse) or 8 (in monkey) sections. Each slide that contained the CeL was imaged with a 40x oil objective with a numerical aperture of 1.3 on a Nikon A1R+ confocal microscope. Stacks were acquired with a z-step of 1.25μm for monkey sections and 1μm for mouse sections and multiple stacks were stitched to produce whole CeL stacks to be used for offline stereological counting. Nikon nd2 files were exported from NIS elements into individual .tif files. Stereological counting was done in StereoInvestigator 2018.1.1 (MBF Bioscience, Williston, VT USA).

A sampling scheme was determined to estimate PKCδ and SST expressing neurons out of total neurons with an estimated Gunderson coefficient of error of 0.1 for each cell type. Neurons were counted when the center of the nucleolus of the NeuN stain came into focus. Cells expressing SST or PKCδ were counted only if they were also double labeled with NeuN. In a pilot study, NeuN and PKCδ+ neurons were counted at 25% in both species and SST+ and double labeled SST/PKCδ neurons were sampled at 100%. Using the sample-resample option in StereoInvestigator it was determined that in both species, PKCδ and NeuN labeled neurons could be sampled at a minimum of 2% and SST neurons could be sampled at a minimum of 10%. To ensure accurate counts, we chose to sample PKCδ and NeuN labeled cells at 5% and SST neurons at 20% in monkey tissue. SST/ PKCδ double labeled neurons were also sampled at 20% in monkey tissue and at 100% in mouse tissue. Section contours were determined based on CeL structure and NeuN staining and also followed the pattern visualized by adjacent AChE stained sections. For cell counting, section thickness was measured at every 10th counting site. Counting frames were set at 75μm x 75μm in both mouse and monkey because frames of this size comfortably contained 4-6 cells. Tissue shrinkage was not consistently observed, and so guard zones were set at 5μm which still allowed for a 30μm disector height. To characterize the A-P distribution of the counted cells, cell counts were divided by the sampling percentage. Counts for each marker were then divided by the number of neurons counted in that section so that they could be presented as percentages.

Overall stereological estimates for each cell type are presented as percentage of the total number of neurons estimated. Between species differences for each cell type were tested using t-tests. Within species and for each cell type, an OLS regression model was used to investigate whether A-P location predicted number of cells counted. A variable for subject was included as a covariate

in this model. A separate OLS model was run to test whether the A-P distribution for each cell type was different between species. One section from one monkey was not used as studentized residuals and cooks distance metrics demonstrated that it was an outlier. All statistical analyses were run in python 3.6 using the statsmodels (version 0.8.0) module.

Surgery Procedure and Tissue Collection for Retrograde Injections

The surgical procedure has been previously described for these animals, which were used as part of other studies (16, 23). The coordinates of the BST were localized for each animal prior to stereotaxic surgery by acquiring T2 weighted (structural) MRI images through the entire brain (3T, coronal sections, 0.8 mm thick, 0.1 mm apart). Animals were pre-anesthetized, intubated, and maintained on isofluorane throughout stereotaxic surgery for placement of injections. We placed multiple small injections (40 nL) of the bidirectional tracers, Lucifer yellow conjugated to dextran amine (LY; 10%, Molecular Probes, Eugene, OR), tetramethylrhodamine, conjugated to dextran amine ('fluoruby', FR; 4%, Molecular Probes), and fluorescein conjugated to dextran amine (FS; 10%, Molecular Probes) into the BSTL, in addition to several injections of the tracer wheat-germ agglutinin-horse radish peroxidase (WGA; 10%, Sigma, St. Louis, MO). Control injections of all tracers were placed in the nearby striatum. Previous studies from our laboratory have indicated that there is no cross-reactivity of antibodies to FR, FS, WGA and LY, permitting injections using different tracers into the same animal.

Two weeks after surgery, animals were deeply anesthetized and perfused through the heart with 0.9% saline containing 0.5 ml of heparin sulfate (200 ml/min for 10 minutes), followed by cold 4% paraformaldehyde in a 0.1 M phosphate buffer/30% sucrose solution (100 ml/min for 1 h). The brain was extracted from the skull, placed in a fixative overnight, and then put through increasing gradients of sucrose (10%, 20%, 30%). Brains were cut on a freezing microtome (40 μm) and all sections were stored in cryoprotectant solution (30% ethylene glycol and 30% sucrose in 0.1 M phosphate buffer) at -20 °C (24). After confirmation of the injection and retrograde labeling using permanent immunostaining methods (23), additional sections through the extended amygdala for each case were selected for triple-labeling experiments.

Retrograde Tracing Imaging Protocol and Analysis

Each slide that contained the CeL was investigated for the density of retrograde-labeled cells. For cases where there were many retrograde-labeled cells, the whole CeL was imaged and multiple stacks were stitched to produce whole CeL stacks to be used for offline counting. In cases where sections only expressed a small number of retrograde-labeled cells, individual stacks centered on the labeled cells were imaged and used for offline counting. Imaging parameters and image handling matched those used above. Retrograde-labeled neurons were first counted with channels for all other markers turned off. Once retrograde-labeled neurons were counted, each channel for the other marker was added to determine co-expression. Cells identified in the top 5μm and bottom 5μm were not counted. The overlap between retrograde-labeled neurons, PKCδ, SST, and SST/ PKCδ are presented as percentages. Venn diagrams were constructed with python 3.6 using the Venn3 module.

Supplemental Results

AT Phenotyping

AT is a composite score of threat-related behavioral and pituitary-adrenal activation occurring during the potentially threatening no eye contact condition (NEC) of the human intruder paradigm (Figure S1A; 1-4). During NEC, monkeys respond by inhibiting their behavior, as characterized by increases in freezing duration and decreases in coo vocalizations. These responses are accompanied by increases in cortisol, a reflection of hypothalamic-pituitary axis activation. AT is calculated within a sample of animals as a standardized composite of NEC-induced increases in freezing duration, decreases in cooing frequency, and increases in plasma cortisol concentration (see above).

To determine whether the AT scores of the 47 animals were representative of the AT scores of a much larger population (n=721) from which the animals in this study were a sub-sample, AT was calculated in two ways. First, AT was determined in relation to the 47 animals used in this study and this was compared to the AT scores of these same animals when calculated with the large group of 721 animals. When examining the AT scores of the animals used in this study as calculated in relation to each other, we found that these AT scores had a similar distribution as the AT scores across the whole 721 animals. AT as calculated within the current sample (n=47), spanned approximately +/- 1 std from the mean of the larger cohort (Figure S1B). We computed the ranks of the AT scores for the 47 animals when they were calculated the two different ways and found that the spearman correlation between the ranks was rho=0.7 ($p<0.0001$). Additionally, a Wilcoxon signed-rank test demonstrated that the ranks did not significantly differ ($Z=527$, $p=0.69$). This demonstrates that the AT scores as calculated within the 47 animals reflects the range of individual differences in the larger population.

CeL Neuronal Collection

Previous work from our laboratory demonstrated that metabolism within the Ce is significantly associated with AT (25, 26). High levels of the serotonin transporter demarcate the CeL so that by imaging the serotonin transporter with positron-emission-tomography, we were able to identify the peak correlation to be within the CeL (Figure S2A; (27). Additionally, neurotoxic lesions of the rhesus Ce result in decreased expression of AT's components (28, 29). These findings in primates, along with rodent studies, formed the basis of our focus on CeL neurons. In the present study, the CeL was identified using acetylcholinesterase staining. In adjacent sections used for LCM, CeL neurons were identified with a neuron-specific rapid staining protocol. This LCM approach was advantageous in specifically identifying the CeL, which changes shape and position across the A-P extent of the amygdala. These CeL neurons were individually captured and pooled, and the RNA was extracted and sequenced (Figure S2B). Across all animals, on average, 90% of the cells that were sequenced were confirmed to have been collected from the CeL, as reflected in our average bregma estimates and CeL neuron accuracy measure for each animal (Table S1, Figure S3B). Neuronal enrichment was also confirmed, as we found greater expression of neuron-specific genes compared to glia-specific genes ($t=36.4$, $p<0.0001$; Figure S3C).

AT's Transcriptomic Architecture

To expand our analyses of the transcriptomic architecture of AT as it relates to its components, we performed four separate regression analyses for each gene's expression level in relation to our phenotypic measures: AT, freezing, cooing, and cortisol. We then asked whether the t-values from each of these regressions between genes and phenotype were correlated across components and AT. Results demonstrated that significant correlations were found between the t-values characterizing the relation between expression levels and AT with the t-values for freezing (Figure S5A, rho=0.88, $p<0.001$), cooing (Figure S5B, rho=-0.72, $p<0.001$), and cortisol

(Figure S5C, rho=0.33, p<0.001). When comparing gene relations among components, we also found associations between genes related to freezing with those related to cooing (Figure S5D, rho=-0.76, p<0.001) as well as between genes associated with cortisol and cooing (rho=0.31, p<0.001, Figure S5E). We did not observe this relationship between genes associated with freezing and cortisol (Figure S5F, rho=-0.02, p=0.27). These data support the hypothesis that AT-related genes include component-general genes such as those that are associated with multiple components and AT rather than a single component, as well as component-specific genes, e.g. those specifically related to freezing.

Weight Gene Co-Expression Network Identifies Gene Modules Associated with AT

Seventy-five modules were identified (Figure S6A; Table S4). Of these, 16 were associated with AT and its components (p<0.05, uncorrected). Of these 10 were AT-related, 5 were associated with freezing, 5 with cooing, and 7 with cortisol (Figure S6B). We also found that 3 modules were AT-specific and 7 which were associated with at least one of AT's component (Figure S6C). Two CeL modules were significantly correlated with AT after multiple testing correction (fdr<0.1) and one of these modules was also significantly correlated with freezing (Figure S6A;). Module P1_I16_M14 has a strong negative association with AT (R^2 = 0.5) and a strong negative association with freezing (R^2 = 0.47). This module was particularly interesting because roughly half of its genes were also found to be associated with AT in our transcript analysis. Module P2_I4_M2 was also significantly and positively associated with AT (R^2 = 0.29) and 56% of the genes comprising this module were also independently associated with AT. Some of the genes within these modules also had high kME scores suggesting that these are "hub" genes that are highly connected to the other genes within the module (Table S4, genes with *).

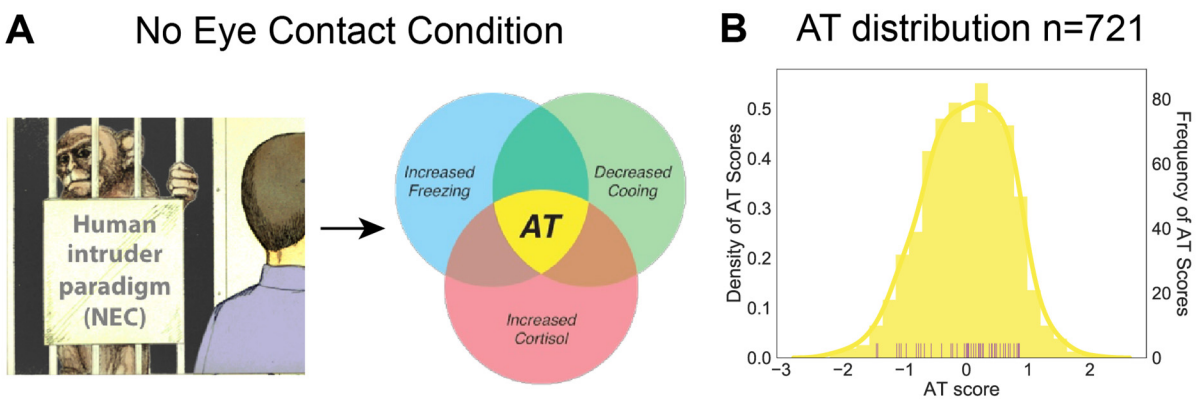

Figure S1. AT phenotype and distribution. (A) Human Intruder No-Eye Contact condition elicits behavioral and physiological responses associated with uncertain threat such as increased freezing, decreased cooing, and increased cortisol, which together comprise the AT-phenotype. (B) Histogram of AT across a larger superset of animals (n=721) in yellow. The purple rugplot below demonstrates the AT scores of the animals in this study as they were calculated within this group of 47 animals.

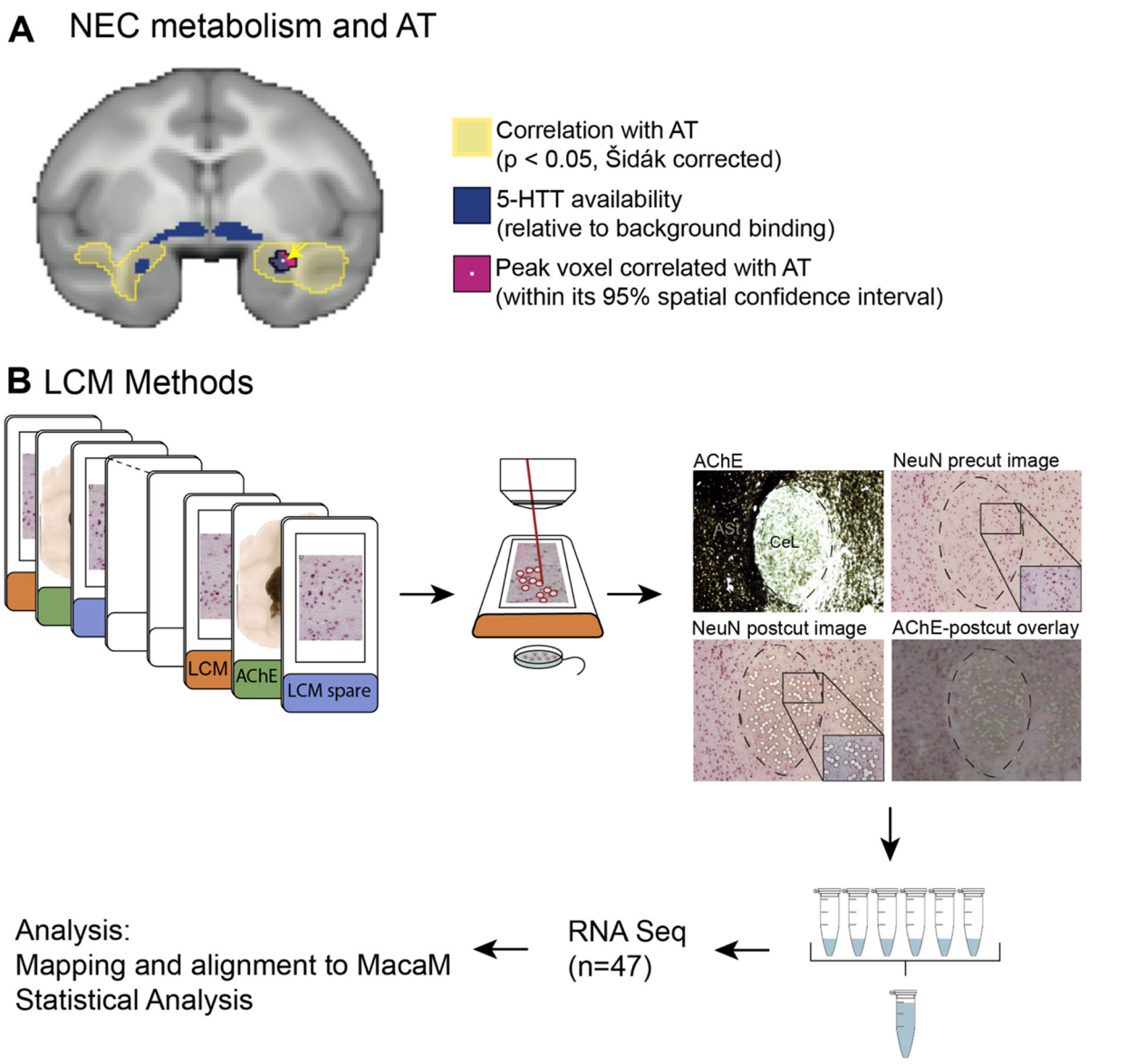

Figure S2. AT-associated PET metabolism in the Ce as a rationale for laser capture microdissection and sequencing of CeL neurons. (A) Using data from our large sample of AT-phenotyped and brain imaged animals, we previously demonstrated that individual differences in NEC-associated PET metabolism are related to individual differences in AT (yellow, (26). We identified the peak AT voxels (pink) to be in the Ce region by demonstrating an overlap with serotonin transporter binding (blue), which, relative to surrounding regions, is elevated in the CeL. (B) Brain slabs containing the amygdala were identified and the A-P location was determined before sectioning. Tissue was sectioned and mounted on LCM slides (orange and blue labels). Adjacent slides were stained with AChE (green labels) to determine the location of the CeL. LCM slides were stained with an abbreviated NeuN protocol and CeL neurons were captured into the lid of a microfuge tube. Post-cut overlays were made for every slide to confirm capture location. RNA from 500-600 CeL neurons was pooled and used for RNA-Seq (n=47). Reads were processed and aligned to MacaM (30).

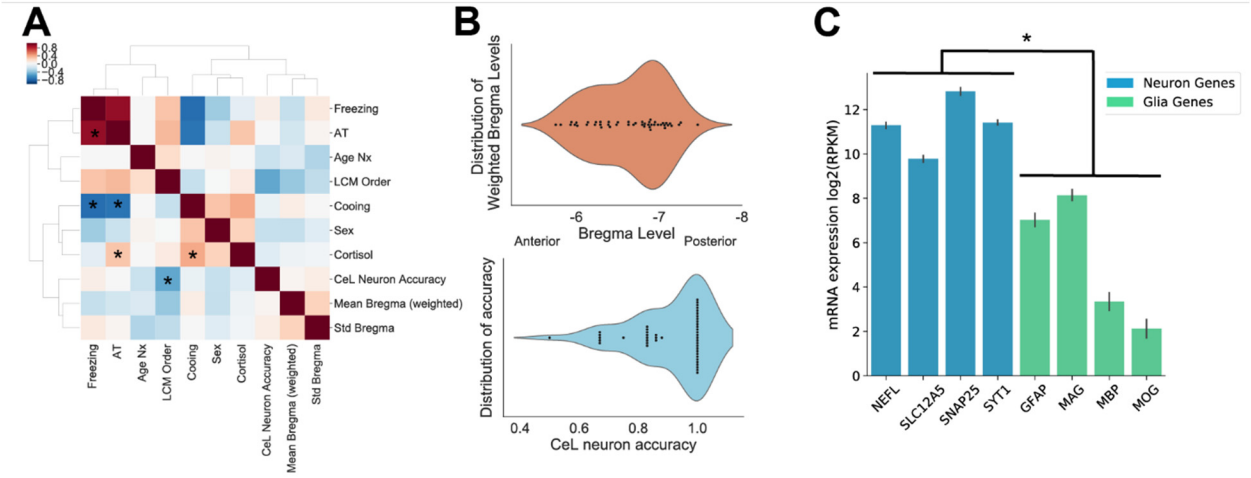

Figure S3. Characterization of LCM sampling method. (A) Heatmap depicting the Pearson correlations between model predictors (AT, freezing, cooing, and cortisol) as well as variables that were tested as covariates. Red indicates a positive correlation. Starred boxes indicate statistically significant Šidák-corrected p-values. (B) Top: Distribution of the weighted average bregma for each animal used for LCM, calculated by multiplying the bregma value of each slide by the number of cells captured in that slide and taking an average for each animal. Bottom: Distribution of CeL neuron accuracy for each animal, calculated as the proportion of the number of slides that contained 80-99% of CeL neurons out of total slides used for RNA-Seq for that animal. (C) Reads per kilobase million (RPKM) normalized mRNA expression values for neuron (blue) and glia (green) associated genes. Neuronal LCM samples expressed on average a greater amount of neuron-specific gene expression than glia-specific gene expression ($p<0.0001$, $t=36.4$; t-test). Error bars are displayed as SEM.

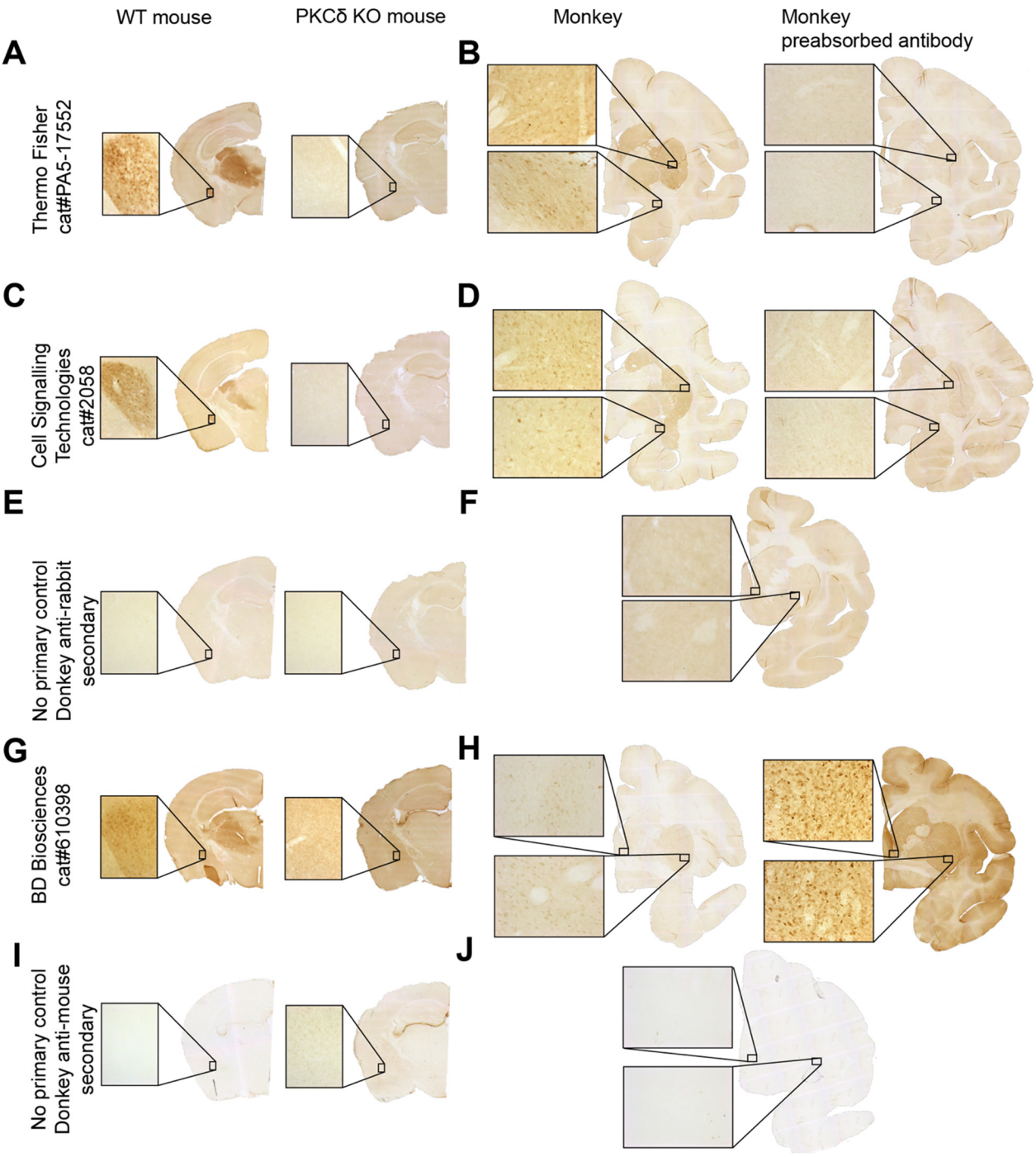

Figure S4. Characterization of PKCδ antibodies. Columns: Wild Type Mouse tissue, PKCδ Knock Out Tissue, Monkey tissue stained with PKCδ antibody, Monkey tissue stained with preabsorbed antibody. Rows: (A-B) ThermoFisher anti-PKCδ antibody, (C-D) Cell Signaling Technology anti-PKCδ antibody, (E-F) Donkey anti-rabbit secondary only control, (G-H) BD Biosciences anti-PKCδ antibody, (I-J) Donkey anti-mouse secondary only control. ThermoFisher and Cell Signaling Technology anti-PKCδ antibodies gave the most robust staining in both monkey and mouse tissue.

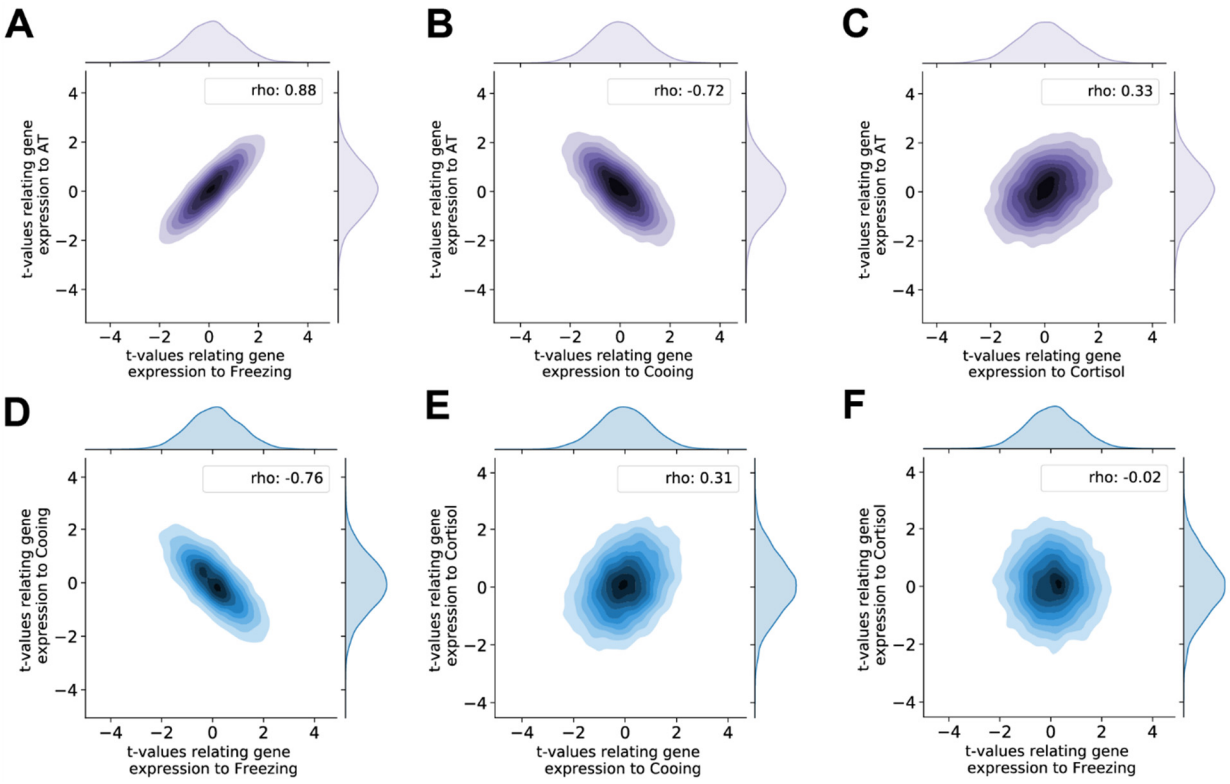

Figure S5. AT components share a molecular substrate. Kernel density plots depicting the distribution of t-values and Spearman correlations between t-values relating gene expression to (A) AT and freezing (rho=0.88, p<0.001) (B) AT and cooing (rho=,-0.72 p<0.001) (C) AT and cortisol (rho=0.33, p<0.001) (D) cooing and freezing (rho=-0.76, p<0.001) (E) cortisol and cooing (rho=0.31, p<0.001) (F) cortisol and freezing (rho=-0.02, p=0.27). Reported p-values are Šidák corrected.

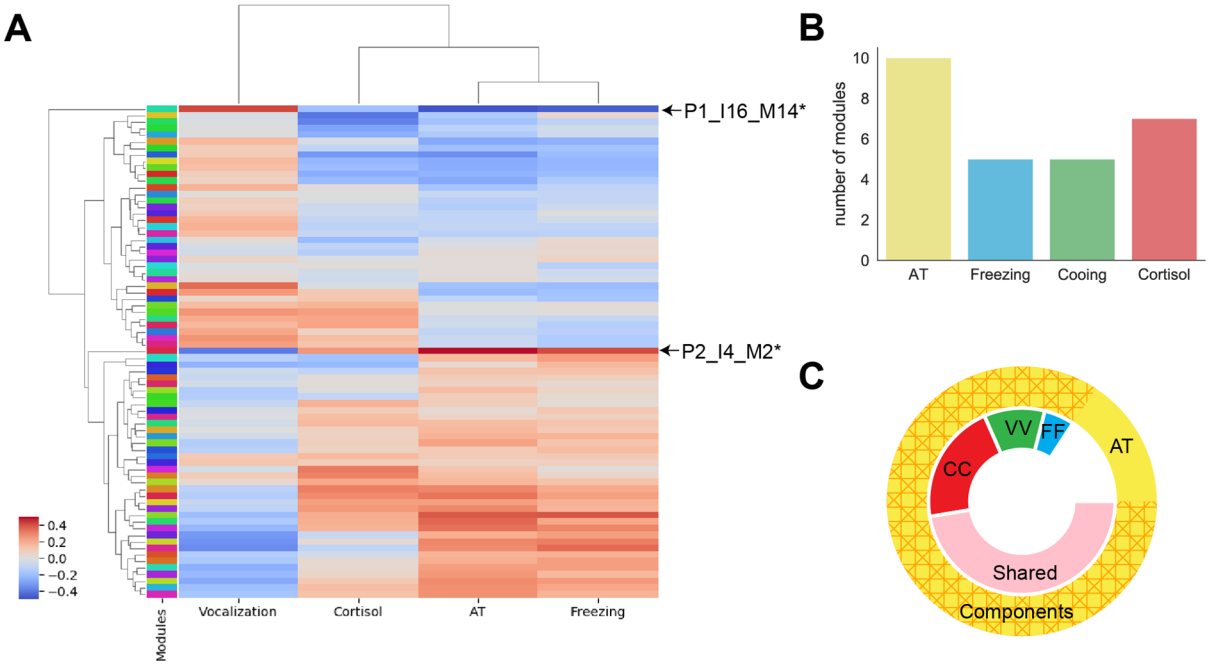

Figure S6. WGCNA modules associated with AT and its components. (A) Heatmap depicting the pearson's correlation between each WGCNA module and AT and its components. Red colors indicate positive correlations and blue colors indicate negative correlations. Two modules (P1_I16_M14 and P2_I4_M2) were significantly associated with AT and passed multiple comparison correction (fdr<0.1). (B) Barplot demonstrating that AT is associated with a greater number of WGCNA modules than each component alone. (C) Donut plot depicting the number of overlapping WGCNA modules between individual AT components and AT. Outside circle represents all AT-associated modules (p<0.05) and is separated into the 13 modules that overlap with AT components (hashed orange) and the 3 modules unique to AT (yellow). Inner circle represents modules that are related to AT and is broken up by modules that are also unique to one AT component (FF: freezing in blue, VV: cooing in green, CC: cortisol in red) or that are shared by at least two components (shared in pink).

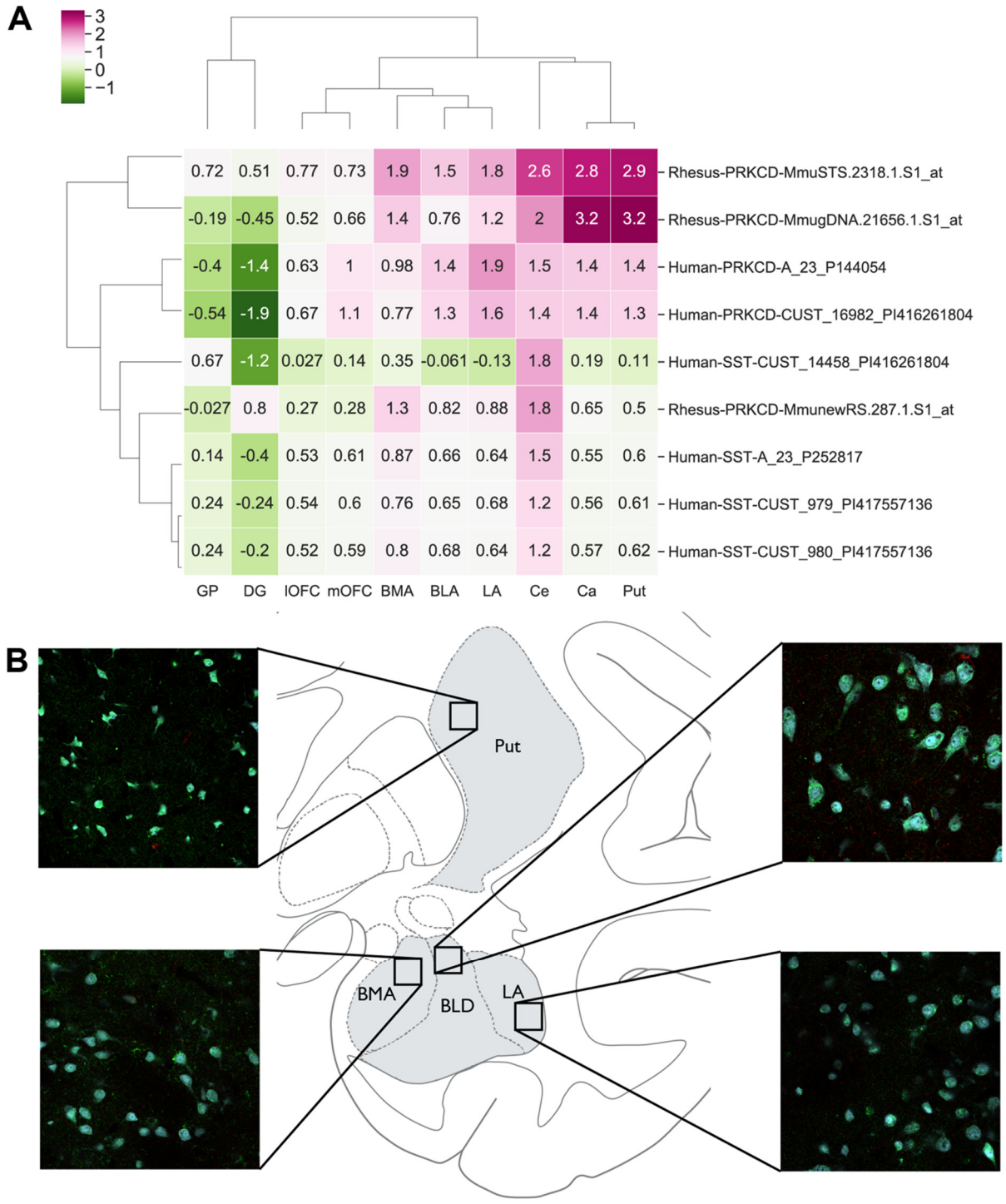

Figure S7. *PRKCD* mRNA and protein is widely distributed throughout the primate brain. (A) A heatmap of the human and nonhuman primate microarray data from the Allen Brain Atlas for *PRKCD* and *SST* demonstrate that the mRNA for these markers are widely distributed throughout multiple brain regions. Particular note is made of high levels of *PRKCD* in the Ce and striatum. The y-axis lists the different microarray probes for each marker for human and nonhuman primate. The x-axis describes the regions of the brain investigated. The color bar depicts the expression values, calculated using a z-score normalization of the relative expression

level of each marker as compared to the rest of the brain (B). Immunofluorescence staining of PKCδ in the putamen as well as other regions of the nonhuman primate amygdala. BLD: dorsolateral division of the basal nucleus of the amygdala, BMA: basomedial nucleus of the amygdala, LA: lateral nucleus of the amygdala, Ce: central nucleus of the amygdala, Ca = caudate, put = putamen, GP: globus pallidus, DG: dentate gyrus of the hippocampus, lOFC: lateral orbitofrontal cortex, mOFC: medial orbitofrontal cortex.

Supplemental References

1. Fox AS, Shelton SE, Oakes TR, Converse AK, Davidson RJ, Kalin NH (2010): Orbitofrontal cortex lesions alter anxiety-related activity in the primate bed nucleus of stria terminalis. *Journal of Neuroscience*. 30:7023-7027.
2. Fox AS, Shelton SE, Oakes TR, Davidson RJ, Kalin NH (2008): Trait-like brain activity during adolescence predicts anxious temperament in primates. *PLoS ONE*. 3:e2570.
3. Kalin NH, Shelton SE, Fox AS, Oakes TR, Davidson RJ (2005.): Brain regions associated with the expression and contextual regulation of anxiety in primates. *Biol Psychiatry*. 58:796-804.
4. Kalin NH, Shelton SE (1989): Defensive behaviors in infant rhesus monkeys: environmental cues and neurochemical regulation. *Science*. 243:1718-1721.
5. Granger FPaBE (2007): IPython: A System for Interactive Scientific Computing. *Computing in Science & Engineering*. 9:21-29.
6. McKinney W (2010): Data Structures for Statistical Computing in Python. *Proceedings of the 9th Python in Science Conference*, pp 51-56.
7. Eric Jones TO, Pearu Peterson, others (2001): SciPy: Open source scientific tools for Python.
8. Seabold S, and Josef Perktold (2010): *Statsmodels: Econometric and statistical modeling with python*.
9. Paxinos G, Huang X, Petrides M, Toga AW (2009): *The Rhesus Monkey Brain: Stereotaxic Coordinates*. Elsevier.
10. Love MI, Huber W, Anders S (2014): Moderated estimation of fold change and dispersion for RNA-seq data with DESeq2. *Genome Biology*. 15:550.
11. Hunter JD (2007): Matplotlib: A 2D Graphics Environment. *Computing in Science & Engineering*. 9:90-95.
12. Greenfest-Allen E, Cartailler J-P, Magnuson MA, Stoeckert CJ (2017): iterativeWGCNA: iterative refinement to improve module detection from WGCNA co-expression networks. *bioRxiv*.
13. Langfelder P, Horvath S (2008): WGCNA: an R package for weighted correlation network analysis. *BMC Bioinformatics*. 9:559.
14. Klopfenstein DV, Zhang L, Pedersen BS, Ramírez F, Warwick Vesztrocy A, Naldi A, et al. (2018): GOATOOLS: A Python library for Gene Ontology analyses. *Scientific Reports*. 8:10872.
15. Kalin NH, Fox AS, Kovner R, Riedel MK, Fekete EM, Roseboom PH, et al. (2016): Overexpressing Corticotropin-Releasing Factor in the Primate Amygdala Increases Anxious Temperament and Alters Its Neural Circuit. *Biol Psychiatry*. 80:345-355.
16. deCampo DM, Fudge JL (2013): Amygdala projections to the lateral bed nucleus of the stria terminalis in the macaque: comparison with ventral striatal afferents. *J Comp Neurol*. 521:3191-3216.
17. Price JL, Russchen FT, Amaral DG (1987): The limbic region. II. The amygdaloid complex. In: Hokfelt BT, Swanson LW, editors. *Handbook of Chemical Neuroanatomy*. Amsterdam: Elsevier, pp 279-381.

18. Atlas AB (2018): Allen Brain Atlas API.: Allen Institute for Brain Science.

19. De Olmos JS (2004): The Amygdala. In: Paxinos G., Mai J.K., editors. *The Human Nervous System* 2ed. San Diego: Elsevier Academic Press.

20. Amaral DG, Price JL, Pitkanen A, Carmichael ST (1992): Anatomical organization of the primate amygdaloid complex. *The Amygdala: Neurobiological Aspects of Emotion, Memory, and Mental Dysfunction*: Wiley-Liss, Inc., pp 1-66.

21. Gundersen HJ (1986): Stereology of arbitrary particles. A review of unbiased number and size estimators and the presentation of some new ones, in memory of William R. Thompson. *Journal of microscopy*. 143:3-45.

22. West MJ, Slomianka L, Gundersen HJ (1991): Unbiased stereological estimation of the total number of neurons in thesubdivisions of the rat hippocampus using the optical fractionator. *The Anatomical record*. 231:482-497.

23. Oler JA, Tromp DP, Fox AS, Kovner R, Davidson RJ, Alexander AL, et al. (2017): Connectivity between the central nucleus of the amygdala and the bed nucleus of the stria terminalis in the non-human primate: neuronal tract tracing and developmental neuroimaging studies. *Brain Struct Funct*. 222:21-39.

24. Rosene DL, Roy NJ, Davis BJ (1986): A cryoprotection method that facilitates cutting frozen sections of whole monkey brains for histological and histochemical processing without freezing artifact. *J Histochem Cytochem*. 34:1301-1315.

25. Fox AS, Oler JA, Shackman AJ, Shelton SE, Raveendran M, McKay DR, et al. (2015): Intergenerational neural mediators of early-life anxious temperament. *Proc Natl Acad Sci U S A*. 112:9118-9122.

26. Oler JA, Fox AS, Shelton SE, Rogers J, Dyer TD, Davidson RJ, et al. (2010): Amygdalar and hippocampal substrates of anxious temperament differ in their heritability. *Nature*. 466:864-868.

27. Shackman AJ, Fox AS, Oler JA, Shelton SE, Davidson RJ, Kalin NH (2013): Neural mechanisms underlying heterogeneity in the presentation of anxious temperament. *Proc Natl Acad Sci U S A*. 110:6145-6150.

28. Kalin NH, Shelton SE, Davidson RJ (2004): The role of the central nucleus of the amygdala in mediating fear and anxiety in the primate. *J Neurosci*. 24:5506-5515.

29. Oler JA, Fox, A.S., Shackman, A.J., and Kalin, N.H. (2016): The central nucleus of the amygdala is a critical substrate for individual differences in anxiety. In Living without an Amygdala. *In Living without an Amygdala*. New York, NY: Guilford Press, pp 218-251.

30. Zimin AV, Cornish AS, Maudhoo MD, Gibbs RM, Zhang X, Pandey S, et al. (2014): A new rhesus macaque assembly and annotation for next-generation sequencing analyses. *Biology Direct*. 9:20.